ORIGINAL ARTICLE

Ionospheric effects on relative positioning within a dense GPS network

S. Lejeune · G. Wautelet · R. Warnant

Abstract Local variability in total electron content can seriously affect the accuracy of GNSS real-time applications. We have developed software to compute the positioning error due to the ionosphere for all baselines of the Belgian GPS network, called the Active Geodetic Network (AGN). In a first step, a reference day has been chosen to validate the methodology by comparing results with the nominal accuracy of relative positioning at centimeter level. Then, the effects of two types of ionospheric disturbances on the positioning error have been analyzed: (1) Traveling ionospheric disturbances (TIDs) and (2) noise-like variability due to geomagnetic storms. The influence of baseline length on positioning error has been analyzed for these three cases. The analysis shows that geomagnetic storms induce the largest positioning error (more than 2 m for a 20 km baseline) and that the positioning error depends on the baseline orientation. Baselines oriented parallel to the propagation direction of the ionospheric disturbances are more affected than others. The positioning error due to ionospheric small-scale structures can be so identified by our method, which is not always the case with the modern ionosphere mitigation techniques. In the future, this ionospheric impact formulation could be considered in the development of an integrity monitoring service for GNSS relative positioning users.

S. Lejeune (✉) · R. Warnant
Royal Meteorological Institute of Belgium, Avenue Circulaire 3, 1180 Brussels, Belgium
e-mail: sandrine.lejeune@oma.be

G. Wautelet
Geomatics Unit, University of Liège, 17 Allée du 6 août, 4000 Liège, Belgium

Introduction

Mismodeling of ionospheric refraction remains a major error source for real-time GNSS applications. Different techniques have been developed to study, understand, model, and mitigate the effects of ionospheric plasma on GNSS signals. One approach uses GPS signals to extract information about ionospheric disturbances. For example, the total electron content (TEC) rate of change computed at a given GPS station is used to detect small-scale structures in electron density (Warnant and Pottiaux 2000; Wautelet et al. 2009). In particular, Wautelet et al. (2009) demonstrated that in mid-latitude regions two main types of ionospheric disturbances can be detected using GNSS systems: (1) Traveling ionospheric disturbances (TIDs) and (2) noise-like variability due to geomagnetic (sub-) storms. These authors show that the probability of TID occurrence is larger during winter months, in particular during daytime. As GPS networks became available, more detailed information on ionospheric disturbances could be observed. For example, Hernandez-Pajares et al. (2006), Tsugawa and Saito (2003) and Saito et al. (2001) are able to extract the direction of propagation, damping, and the wavelength of large-scale TIDs (LSTIDs) by using TEC measurements over GPS networks. The comparison of TEC at different stations is also used to understand the propagation of geomagnetic storms and sub-storms in the complex thermosphere–ionosphere system (Mayer et al. 2008; Gomez et al. 2007).

In another approach, the influence of the ionosphere, particularly the small-scale structures, on positioning has been analyzed (Mohino 2008; Gende et al. 2005). Such

studies try to estimate which part of the positioning error is due to the ionosphere for a given epoch. The effect of the ionosphere on real-time relative positioning has also been studied. Most of the studies aimed either to develop mitigating techniques to improve the precision at short distance (Wanninger 1999; Ou and Wang 2004) or to maximize baselines lengths within a network of stations for a given accuracy level (Chen et al. 2004; Hernandez-Pajares et al. 2000). The current most prevalent methods which rely on a network of continuously operating reference stations (CORS) are the VRS (Virtual Reference Station) and the MAC (Master-Auxiliary Concept) approaches. Those technologies (VRS, FKP—in German *Flächenkorrekturparmeter* and MAC) use dense GNSS networks to improve the ionospheric error modeling. They thus offer highly accurate positioning over distances of several tens of kilometers (Janssen 2009). However, studies of these contemporary positioning methods such as those of Brown et al. (2005, 2006) and Janssen (2009) compare accuracies without giving any information regarding the ionospheric contribution to the error budget.

We are specifically interested in the ionospheric impact on dense networks and therefore focus on monitoring and quantifying the contribution of ionospheric disturbances to the classic relative positioning error budget. Our research does not aim at improving the precision of relative positioning but seeks to underline the limitations of dense networks to deal with ionospheric disturbances. We have chosen to analyze classic Real-Time Kinematic (RTK) as a preliminary step before considering modern techniques like VRS, FKP, or MAC. In conventional single-base RTK, the moving receiver determines its relative position with respect to a reference station whose position is known with high accuracy. If the stations are not too far apart, the ionospheric residual term is generally assumed to be negligible. This assumption can be verified during quiet ionospheric conditions, which means that no local variability in TEC is observed. Indeed, as long as ionospheric conditions remain quiet, the nominal accuracy of the relative positioning technique is reached (Wanninger 1999; Hofmann-Wellenhof et al. 2001; Vollath et al. 2002; Leick 2004), meaning centimeter-level accuracy for the North, East, Up components. In the presence of ionospheric small-scale irregularities, the ionospheric residual term tends to be not negligible and acts on GNSS processing software in two ways. On the one hand, ambiguity resolution can fail or ambiguities are fixed to the wrong integer value, which can lead to positioning errors up to one meter for baselines as small as 4 km (Lejeune and Warnant 2008). This problem also surfaces in post processing when the observation session is too short. On the other hand, even after successful ambiguity resolution, if the ionospheric error is not taken into account in the least-squares model, it affects the estimation of the user

position. As a solution, an appropriate way to obtain ionospheric-free positions is to consider the ionospheric error as an additional unknown. The residual ionosphere is then considered a separate part of the model. Such ionospheric mitigation techniques are beyond the scope of this article. In this research, we assume that users have already fixed their ambiguities to the true integer values. We developed the software SoDIPE-RTK (Software for Determining Ionospheric Positioning Error on RTK) which runs on a network of reference stations whose positions are known. For each day and each epoch, this post-processing software allows for the computation of ambiguities and positioning error due to the ionosphere for all the 160 baselines of the Active Geodetic Network (AGN). In our research, only GPS data are processed. However, the proposed method could be applied to any other GNSS system.

First, we present the methodology implied in software and data selection. The validity of the method is tested by processing a day with quiet ionospheric conditions. Next, we analyze the effects of baseline length and orientation on positioning error during disturbed ionospheric conditions. Finally, results are discussed and several perspective areas of research are proposed.

Methodology

The SoDIPE-RTK software detailed in this section uses RINEX observation and navigation files to compute the positioning error due only to the ionosphere for a given baseline. It runs in a post-processing mode.

Software development

Our software processes GNSS data in three main steps. The first one consists in forming double differences like in classic RTK. Then, using geometry-free phase combination, we compute the differential ionospheric effect, which is used in the third step to extract the ionospheric positioning error.

Double differences

In relative mode, RTK users combine their own phase measurements (mobile station B) with measurements made by a reference station (A) for which the position is known. The basic observable is called double difference (DD) of phase measurement. In a first step, SoDIPE-RTK computes DD for every epoch and every carrier. The sample rate is 30 s for the data used in this study. If $\phi_{A,k}^i$, $\phi_{B,k}^i$, $\phi_{A,k}^j$, and $\phi_{B,k}^j$ are the four undifferenced phase measurements between receivers A, B and satellites i, j, on carrier L_k, the double difference $\phi_{AB,k}^{ij}$, expressed in meters, is computed as follows,

$$\phi_{AB,k}^{ij} = (\phi_{A,k}^i - \phi_{B,k}^i) - (\phi_{A,k}^j - \phi_{B,k}^j)$$
$$= D_{AB}^{ij} - I_{AB,k}^{ij} + T_{AB}^{ij} + M_{AB,k}^{ij} + \lambda_k N_{AB,k}^{ij} + \varepsilon_{AB,k}^{ij} \quad (1)$$

with λ_k is the wavelength, D_{AB}^{ij} is the double-difference geometric term, $I_{AB,k}^{ij}$ is the ionospheric residual term, T_{AB}^{ij} is the tropospheric residual term, $M_{AB,k}^{ij}$ is the multipath term, $N_{AB,k}^{ij}$ is the ambiguity term, and $\varepsilon_{AB,k}^{ij}$ is the noise.

Differential ionospheric effect

In a second step, we extract the ionospheric residual term by computing the geometry-free phase combination $\phi_{AB,GF}^{ij}$. Indeed, neglecting multipath and noise, we obtain from (1),

$$\phi_{AB,GF}^{ij} = \phi_{AB,L1}^{ij} - \phi_{AB,L2}^{ij}$$
$$= \alpha STEC_{AB}^{ij} - \lambda_k N_{AB,GF}^{ij} \quad (2)$$

with $\alpha = 40.3(\frac{1}{f_2^2} - \frac{1}{f_1^2})$, f_1 and f_2 are the GPS frequencies and $STEC_{AB}^{ij}$ is the combination of the four slant TEC values. For each DD, the float ambiguity $N_{AB,GF}^{ij}$ is solved using the whole observation period, so that the process cannot be considered as a real-time one. After ambiguity resolution, $STEC_{AB}^{ij}$ can be computed to reconstruct the ionospheric residual term $I_{AB,k}^{ij}$ on each GPS carrier k,

$$I_{AB,k}^{ij} = 40.3 \frac{STEC_{AB}^{ij}}{f_k^2} \quad (3)$$

Based on this ionospheric residual reconstruction, we can compute the positioning error due to the ionosphere.

GPS–RTK positioning error due to the ionosphere

The three components of the RTK positioning error (North, East, and Height) are computed for every epoch using a least-squares adjustment of L_1 DD carrier phase observations (1). The positioning method in SoDIPE-RTK is therefore based on single-frequency measurements, but uses ambiguities $N_{AB,GF}^{ij}$ estimated previously from dual-frequency measurements. The L_1 carrier was chosen because it offers more precise and reliable observations than L_2.

The least-squares adjustment is based on regular carrier phase observation equations. The estimate for the unknowns is represented in the familiar matrix–vector notation as,

$$\underline{x} = (A^T P A)^{-1} A^T P \underline{l} \quad (4)$$

with $\underline{l}$ being the vector of observations, A is the design matrix containing partial derivatives, $\underline{x}$ is the vector of

unknowns representing the three components of the positioning error, and P is the weight matrix.

In our study, the permanent GPS stations serve as reference station (A) and as user (B), so that the position of these stations is known with sub-centimeter accuracy. Since the nominal RTK accuracy is usually a few centimeters, we will further consider that the positions of the permanent stations are perfectly known and we will refer to them as the true positions. As a consequence, D_{AB}^{ij} which appears in (1) is a known quantity, and the unknowns $\underline{x}$ depend on all other error sources contained in this equation such as multipath, troposphere, ionosphere, and noise, except for the ambiguities, which have been previously solved and corrected for. Since we are only interested in ionospheric effects on positioning error, we can simply express the vector of observations as follows:

$$l_{AB,k}^{ij}(t) = -I_{AB,k}^{ij}(t) \quad (5)$$

The positioning error resulting from the least-squares adjustment is, in this manner, only affected by the ionospheric residual term, referred below simply as the "positioning error", and can be expressed in three components (ΔN, ΔE, and ΔH). We computed also the positioning error in terms of distance ($\Delta B = \sqrt{\Delta N^2 + \Delta E^2 + \Delta H^2}$). The influence of multipath and noise on I_{AB}^{ij}, and therefore on positioning error, will be assessed on quiet ionospheric conditions during the validation phase of the methodology.

Data selection

The AGN consists of 66 dual-frequency GPS stations operated by three different institutions: FLEPOS (Flemish part, 40 stations), WALCORS (Walloon part, 23 stations), and the Royal Observatory of Belgium, ROB (3 stations). FLEPOS started in October 2002, WALCORS in September 2003, while the ROB stations have been operational since the 1990s.

Since we are dealing with relative positioning, we have to form baselines between these 66 receivers. In order to assure that all triangles of stations are as much as possible equilateral, a common approach in selecting the baselines is Delaunay triangulation. Since RTK networks are usually designed for the use of VRS and MAC techniques, the rover and reference stations are practically not separated by more than 25–30 km. In our study, we decided to select all baselines less than 40 km. The total number of baselines created by the Delaunay triangulation which are less than 40 km is 161 (Fig. 1). The mean baseline length in the AGN is 24.7 km, while 95% of the baselines are less than 36.1 km. There is a slight difference in density between the
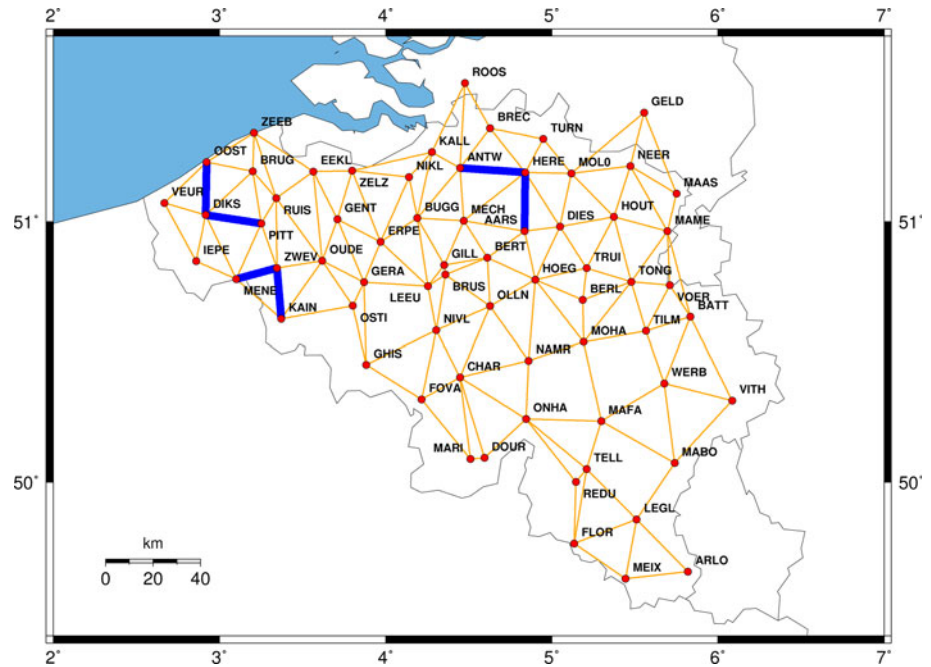
sub-networks FLEPOS and WALCORS with a mean
baseline length of 23.5 and 28.7 km, respectively.

In order to identify the effects of ionospheric structures
on relative positioning, three particular days, based on their
typical ionospheric conditions, were analyzed in detail.

DOY 310/2008: a quiet day

We selected November 5, 2008, as a reference day (Fig. 2).
This day is characterized by a quiet TEC background of less
than 10 TECU and quiet geomagnetic activity with *Kp*
value of 0.3. Furthermore, nearly no ionospheric events
were detected by the single-station method developed by
Warnant and Pottiaux (2000). This technique allows
detection of small-scale structures in ionospheric plasma by
analyzing the geometry-free combination at a given GPS
station. When variability is present, the method detects a so-
called ionospheric event with an associated intensity, called
"RTK intensity". DOY 310/2008 is therefore considered as
representative of a quiet ionosphere.

DOY 359/2004: a typical MSTID

While the occurrence of medium-scale TID is relatively
common around noon in winter (Fig. 3), we chose the day
for which the intensity of the events presents the largest
values. On December 24, 2004, the MSTID occurred from
9 a.m. to approximately 3 p.m. Maximal value of rate of
TEC or RoTEC, which is the TEC time derivative, was
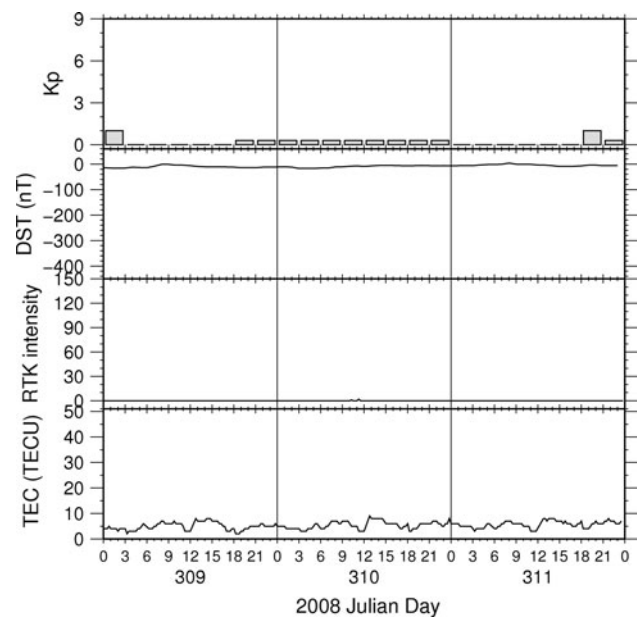about 0.8 TECU/min around noon at BRUS. As this kind of

Fig. 2 Geomagnetic and ionospheric context for DOY 310/2008

TID is generally not linked to geomagnetic activity, the
geomagnetic indices for this day show, as expected, very
quiet conditions ($Kp_{max} = 2$ and $DST_{min} = -26$ nT). The
background TEC for DOY 359/2004 is also quiet, with a
maximum of about 10 TECU, which corresponds to solar
quiet conditions (monthly sunspot number Rd $= 17.9$). As
the TID occurred between 9 a.m. and 3 p.m., we will only
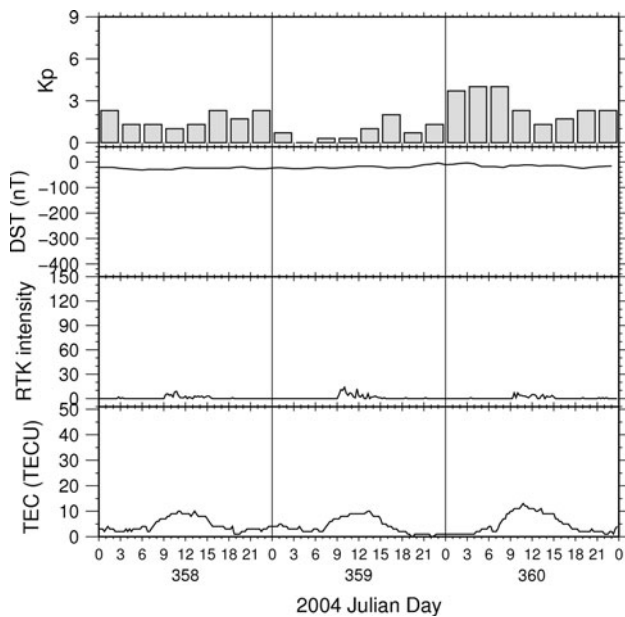consider this time period in further computations.

Fig. 3 Geomagnetic and ionospheric context for DOY 359/2004

Fig. 4 Geomagnetic and ionospheric context for DOY 324/2003

DOY 324/2003: a powerful geomagnetic storm

On November 20, 2003, a huge coronal mass ejection coming from a giant sunspot group hit the earth's magnetosphere, which led to a severe geomagnetic storm, as shown in Fig. 4. It was one of the most powerful geomagnetic storms ever observed since the beginning of GPS recording. Indeed, DST values reached −422 nT around 8 p.m., while the *Kp* index was 8.7 over 6 h. The ionospheric background of DOY 324/2003 was relatively high, partially due to the large value of the sunspot number (Rd = 67.3): a maximum of about 50 TECU was observed around noon, which represents +150% of the TEC background of the previous day. A secondary maximum of about 30 TECU was also observed around 8 p.m., in phase with a large increase of RTK intensity and increasing geomagnetic activity. The maximum RoTEC value at BRUS was about 9 TECU/min at 7 p.m. Since the effects of the geomagnetic storm began to increase after 3 p.m., see RTK intensity values in Fig. 4, we will only consider the data relative to the time interval [3 p.m.–12 p.m.] in further computations.

Results

In order to assess the ionospheric effects on positioning error under disturbed conditions, it is crucial to have a reference data set where positioning errors due to the ionosphere have been computed under quiet ionospheric conditions. As a firs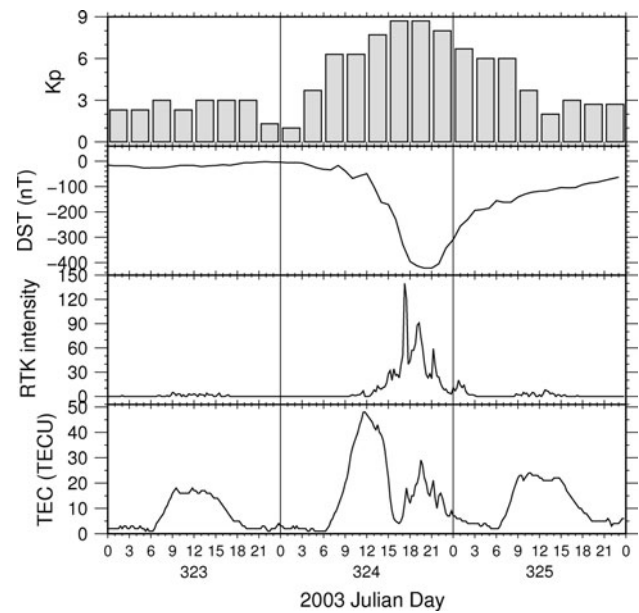t step, this section thus provides the results related to the AGN nominal accuracy. Then, we focus on the analysis of the effect of ionospheric disturbances.

Characterization of the AGN nominal accuracy

The reference data set will be used to validate the present technique and to decide when non-nominal conditions occur. Moreover, we study the AGN nominal positioning conditions to answer two questions: (1) is the influence of residual ionosphere still negligible when increasing the baseline length and (2) is there a maximum usable length?

We compute all AGN baselines to extract the ionospheric residual term on DD and the positioning error, that is 3 components and ΔB. All baselines containing residual cycle slips, data gaps, and outliers have been filtered out manually from the data set. For DOY 310/2008, which has been chosen as the quiet reference day, the number of appropriate baselines dropped from 146 to 131. This means that about 10% of the baselines were problematic and were therefore removed from the results. Then, we compute per baseline the daily average ($\bar{x}$) and standard deviation (σ) for each component and for ΔB (Fig. 5). Since the sampling rate is 30 s, the number of observations for each baseline is 2,880.

In order to analyze the relationship between $\bar{x}$ or σ as a function of baseline length, we compute statistical linear regressions between these variables. Since the baseline length is known within a few millimeters, we assume that there is no error in this parameter and considered it as the independent variable. On the contrary, the $\bar{x}$ and σ values
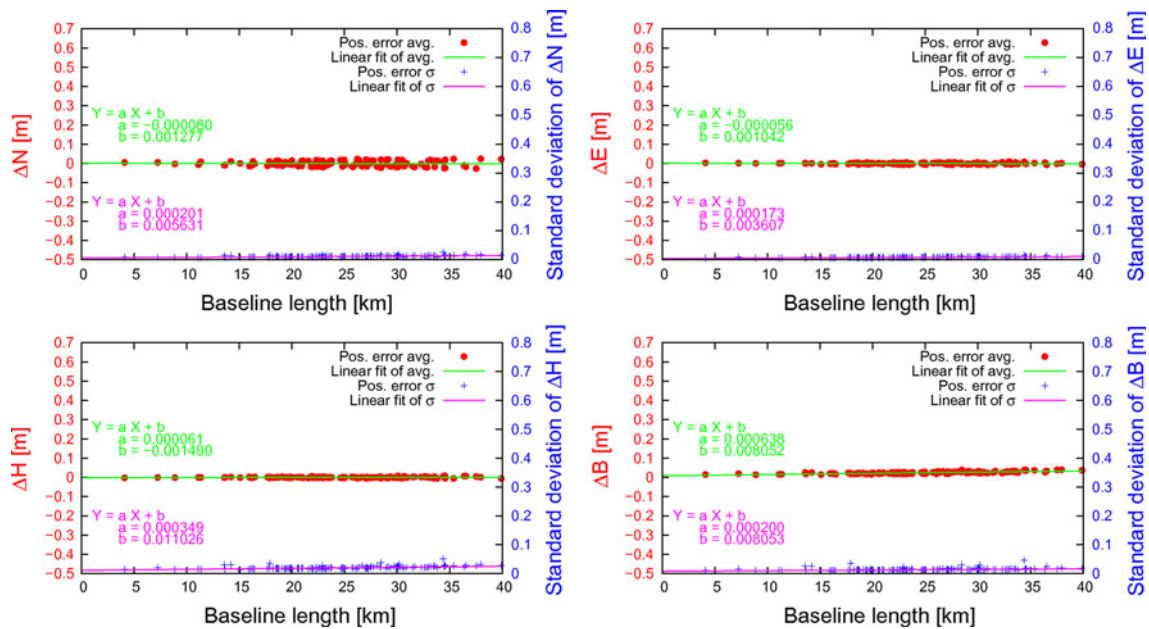
Fig. 5 Positioning error as a function of baseline length for DOY 310/2008 (whole day). The three components North (ΔN), East (ΔE), and Height (ΔH) and distance (ΔB) are plotted for average ($\bar{x}$) and standard deviation (σ) values

cannot be considered as perfect measurements, so that linear regression on both the variables will be computed considering the variance on the measurements in a weighted least-squares fit. The slopes of regression lines relative to $\bar{x}$ (Fig. 5) are very close to zero for ΔN, ΔE, and ΔH, while the slope relative to ΔB seems to be positive. To confirm these assumptions and prove whether the slopes are statistically null, we realized statistical tests on linear regressions. These tests have been performed for a significance level $\alpha = 0.1\%$ and confirm our hypotheses: ΔN, ΔE, and ΔH slopes are null, while the one for ΔB is not. The same analysis has been used for the slopes relative to σ values (Fig. 5); the statistical tests prove that they are all significantly positive. Therefore, one can summarize the results as follows: for the three components, $\bar{x}$ does not increase with baseline length, while σ does. In other words, residual ionosphere in DD results in a larger variability on positioning error, but does not induce any bias. This conclusion is not valid for ΔB that shows a positive trend with baseline length for both $\bar{x}$ and σ.

As previously stated and is well known, the multipath effect and measurement noise contribute both to the positioning error; it is therefore important to isolate these effects from the ionospheric one. Since multipath and noise are not spatially correlated, the magnitude of their effects would not depend on baseline length. However, we have statistically proved for this data set that the positioning error variability increases with baseline length. It strongly suggests that regression slopes are due to the ionosphere, and more particularly to the spatial decorrelation which

increases with baseline length, and not due to multipath and measurement noise. These observations and this analysis therefore validate the methodology used in this research.

From a numerical point of view, we can see that the slope of the regression line relative to σ is 0.2 mm/km or 0.2 ppm for ΔE and ΔN, whereas it reaches 0.4 ppm for ΔH. For the quantity ΔB, the value of σ equals 0.2 ppm, which is one half the value of ΔH. This is easily explained by the fact that all ΔB values are always positive. We therefore can say that ΔB is not really the representative of the effects on each component, but constitutes a synthetic index to quantify and compare the different trends and effects. Considering that the typical relative positioning accuracy, as in case of RTK, is of the order of 1 cm for each component, we can see that this limit is reached for a 50-km baseline in both ΔN and ΔE components and for a 25-km baseline for the ΔH component. This means that, considering a centimeter-level accuracy, the influence of the ionosphere can be neglected during quiet conditions if the baseline length does not exceed 25 km. This length of 25 km can therefore be considered as the maximum usable length for relative positioning, while assuming $\sigma = 1$ cm on each component. The use of this σ value means that about 67% of the measurements are within $[\bar{x} \pm \sigma]$. If the centimeter-level accuracy has to be achieved in 95% of cases, we must consider the confidence interval $[\bar{x} \pm 1.96\sigma]$. Therefore, the maximum baseline length has to be reduced by a factor 2. That means that the maximum usable length, considering $\sigma = 1$ cm for all components in 95% of cases, is about 13 km. These results complete the validation of the methodology. Indeed,
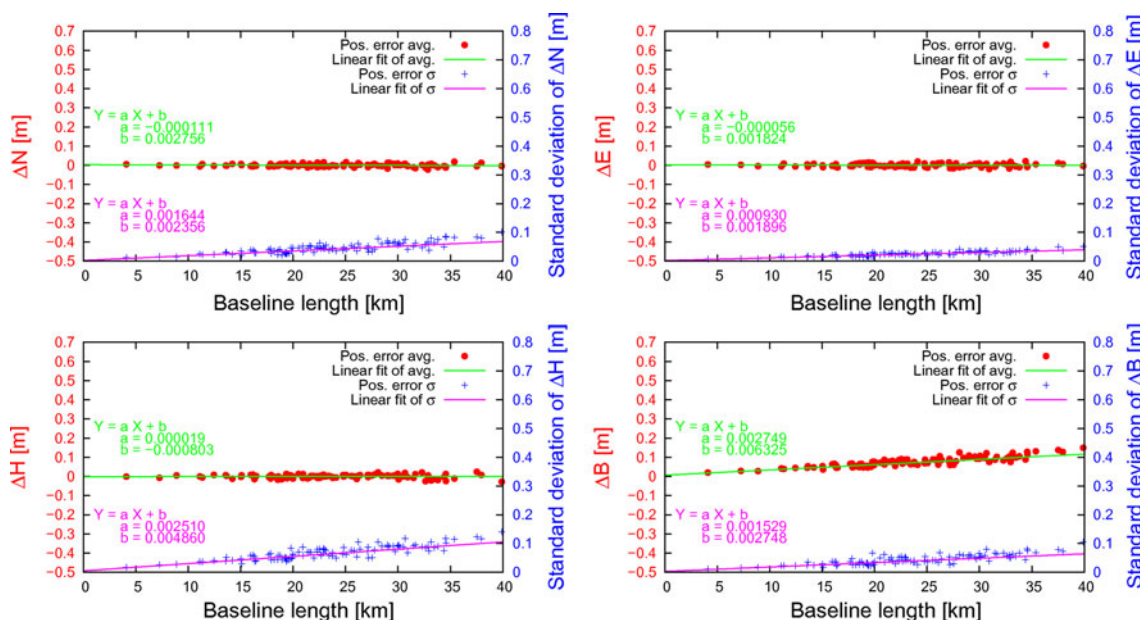
Fig. 6 Positioning error as a function of baseline length for DOY 359/2004 (from 9 a.m. to 3 p.m.). The three components North (ΔN), East (ΔE), and Height (ΔH) and distance (ΔB) are plotted for average ($\bar{x}$) and standard deviation (σ) values

the σ values obtained for each component and the maximum usable length are of the same order of magnitude that the nominal conditions currently admitted by the relative positioning technique users.

Effect of ionospheric small-scale disturbances on precise relative positioning

We analyzed the influence of the baseline length during disturbed conditions. Moreover, we investigated the effect of the baseline orientation on positioning error to highlight a potential influence of the direction of propagation of ionospheric disturbances. Finally, our results are compared to another existing ionospheric index called I_{95} (Wanninger 1999).

Effect of baseline length

The same procedure as the one described in the previous section for DOY 310/2003, has been used to study the effect of baseline length on two other days. We only analyzed for those 2 days disturbed ionospheric periods, which are [9 a.m.–3 p.m.] for DOY 359/2004 (MSTID) and [3 p.m.–12 p.m.] for DOY 324/2003 (geomagnetic storm).

DOY 359/2004: As with quiet conditions, the analysis of $\bar{x}$ values of DOY 359/04 shows no significant trend of the positioning error for the three components, the slopes of the regression being non-significantly different from zero (Fig. 6). However, for a similar baseline length, residuals of the regression are generally larger during the TID

occurrence than during the quiet reference day DOY 310/08. This increased variability around the regression line, not linked to the baseline length, could be understood as an effect of baseline orientation. This hypothesis will be tested in the next section.

When analyzing the σ values, we can observe and confirm statistically that the variability on positioning error increases significantly with baseline length for all components, including ΔB. From a numerical point of view, one can observe that the residual ionospheric error is responsible for 1.5 ppm variability for ΔN, 1 ppm for ΔE, 2.5 ppm for ΔH, and 1.5 ppm for ΔB. Once again, the largest value is obtained for the Height component, while the smallest is the East component. Under such circumstances, centimeter-level accuracy is reached for a baseline not longer than 4 km, considering the variability on the Height component with a 67% confidence interval. If $\sigma = 1$ cm has to be achieved in 95% of cases, the maximum usable length in this context drops to 2 km.

DOY 324/03: When looking at Fig. 7, the conclusions are quite similar to the previous ones, namely (1) an increasing variability with the baseline length and (2) no bias for the average positioning error. Nevertheless, residuals are much larger during the geomagnetic storm than during the TID and the quiet reference day. Numerical values of the variability on positioning error are 3.5, 2.5, 6.5, and 5.5 ppm, respectively, for ΔN, ΔE, ΔH, and ΔB. On this basis, the maximum baseline length for centimeter-level accuracy in 67% of cases is less than 2 km. This value drops to about 1 km considering a 95% confidence interval.
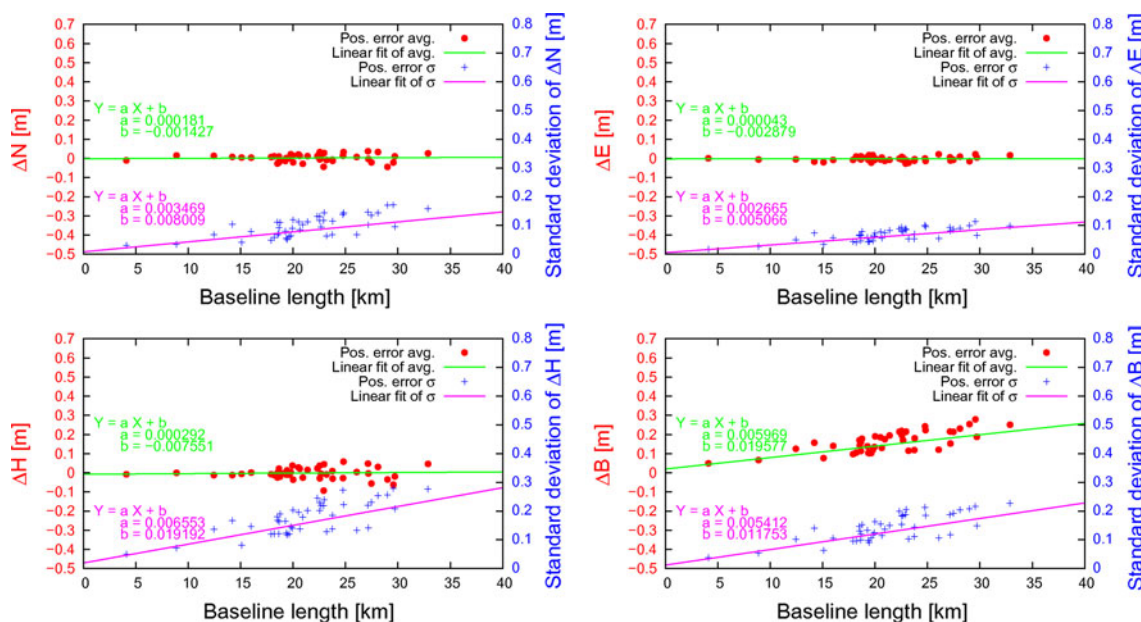
Fig. 7 Positioning error as a function of baseline length for DOY 324/2003 (from 3 p.m. to 12 p.m.). The three components North (ΔN), East (ΔE), and Height (ΔH) and distance (ΔB) are plotted for average ($\bar{x}$) and standard deviation (σ) values

Effect of baseline orientation

In order to analyze the effects of baseline orientation, we produce polar plots for each selected day (Fig. 8), where σ of the ΔB component ($\sigma_{\Delta B}$) is plotted as a function of baseline azimuth. Since we want to compare all baselines with each other, it is necessary to eliminate the length effect. Therefore, $\sigma_{\Delta B}$ has been normalized by the baseline length. As for the previous section, polar plots contain all AGN baselines showing neither gap, nor residual cycle slip. For DOY 310/08, the $\sigma_{\Delta B}$ values are for each baseline rather low and almost isotropic. Contrary to this day, the $\sigma_{\Delta B}$ values of DOY 359/04 show an influence of baseline orientation on the positioning error. Indeed, the polar plot

shape presents a north–south preferential orientation: this direction is generally affected by errors larger than others. This orientation effect is also clearly visible for DOY 324/03. Moreover, the value of the radius, mostly larger than 6 ppm, also confirms that the impact of a geomagnetic storm on positioning error is larger than the effect of a typical MSTID.

In order to investigate further the impact of the baseline orientation, the analysis of these polar plots will be completed by detailed case studies. For this purpose, three pairs of baselines sharing one common station were chosen to form small sub-networks (Fig. 1). These pairs are roughly characterized by the same length, but have different orientation, which have been chosen north–south and
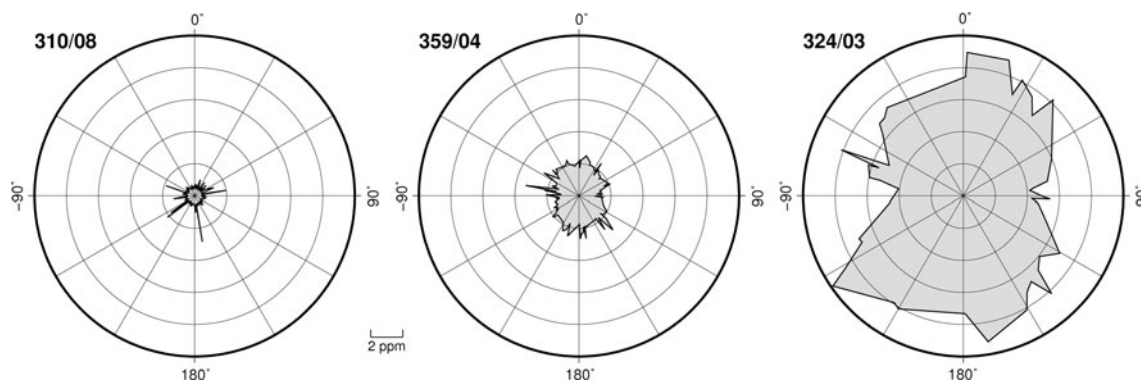

Fig. 8 Standard deviation of distance (ΔB) component normalized by the baseline length (ppm) for DOY 310/2008, DOY 359/2004 (from 9 a.m. to 3 p.m.), and DOY 324/2003 (from 3 p.m. to 12 p.m.) for all AGN baselines

Table 1 SD and MAX values for the various AGN baselines selected

Baseline	Dist (km)	Day	Period	North (m)		East (m)		Height (m)		Distance (m)	
				SD	MAX	SD	MAX	SD	MAX	SD	MAX
AARS-HERE N–S	24.81	310/2008	Day	0.012	0.033	0.008	0.025	0.020	0.084	0.013	0.014
		359/2004	9–15h	0.047	0.114	0.029	0.071	0.086	0.268	0.054	0.278
		324/2003	15–24h	0.143	0.686	0.095	0.552	0.221	1.936	0.184	2.069
ANTW-HERE W–E	27.53	310/2008	Day	0.013	0.048	0.009	0.021	0.021	0.079	0.014	0.100
		359/2004	9–15h	0.034	0.116	0.021	0.034	0.051	0.139	0.029	0.160
DIKS-OOST N–S	22.32	310/2008	Day	0.010	0.030	0.007	0.030	0.019	0.085	0.012	0.124
		359/2004	9–15h	0.046	0.128	0.027	0.075	0.071	0.199	0.042	0.251
		324/2003	15–24h	0.136	0.864	0.083	0.497	0.239	1.809	0.199	2.061
DIKS-PITT W–E	23.74	310/2008	Day	0.010	0.052	0.007	0.035	0.021	0.150	0.016	0.159
		359/2004	9–15h	0.041	0.142	0.019	0.047	0.057	0.185	0.034	0.195
		324/2003	15–24h	0.067	0.389	0.053	0.186	0.142	0.914	0.115	1.303
KAIN-ZWEV N–S	21.71	310/2008	Day	0.011	0.035	0.009	0.066	0.020	0.129	0.017	0.137
		359/2004	9–15h	0.051	0.176	0.028	0.069	0.069	0.228	0.040	0.236
MENE-ZWEV W–E	17.89	310/2008	Day	0.008	0.033	0.006	0.019	0.015	0.093	0.009	0.094
		359/204	9–15h	0.027	0.066	0.016	0.034	0.042	0.111	0.025	0.152
		324/2003	15–24h	0.048	0.299	0.042	0.146	0.121	0.769	0.096	0.830

east–west. They are : (a) AARS-HERE (25 km) and ANTW-HERE (28 km), (b) DIKS-OOST (22 km) and DIKS-PITT (24 km), and (c) KAIN-ZWEV (22 km) and MENE-ZWEV (18 km), respectively. These baselines form a set of triangles required in the computation of the I_{95}-index, allowing a direct comparison with the results of SoDIPE-RTK. Maximum (MAX) and σ values of positioning error relative to these triangles of stations are given in Table 1.

DOY 310/2008: Table 1 shows that σ varies between 0.006 m and 0.021 m, depending on the component. As for the effect of baseline length, the East component presents the lowest values, while the Height component shows the largest. No clear effects of baseline orientation can be found since σ differences between baselines are within the same order of magnitude than measurement noise for a given component. In conclusion, one cannot state that there is any effect of baseline orientation on positioning error for this particular day.

DOY 359/2004: The σ values are at least two times larger for this day than for DOY 310/2008 (Table 1). Moreover, they confirm the influence of baseline orientation previously observed in the polar plots. Indeed, the σ and MAX values for baselines with a north–south orientation: (a) AARS-HERE, (b) DIKS-OOST, and (c) KAIN-ZWEV are, for each component, larger than those obtained for other baselines (east–west orientation). These numerical observations are also presented for AARS-HERE and ANTW-HERE in Fig. 9. Even though the error values are similar during most of the day, it is not the case during the TID occurrence between 9 a.m. and 3 p.m. During this

period, a maximum value of 0.278 m is observed for AARS-HERE (north–south orientation), while ANTW-HERE baseline reaches simultaneously a maximum value of 0.160 m. Since the difference cannot be attributed to the length difference of 2.7 km between the two baselines, it suggests that such effect is due to the direction of propagation of the TID. In theory, a planar wave propagating in a given direction induces a smaller TEC gradient for a baseline oriented parallel to the wave front than for a perpendicular one. Since in the northern hemisphere, the MSTIDs propagate mostly southward or southeastward during the winter (Hernandez-Pajares et al. 2006), one can therefore assume that baselines with east–west orientation would experience smaller errors than north–south ones. To get more information about the ionospheric small-scale structures propagation, we can also observe the RoTEC in the various stations. RoTEC for satellite PRN17 is for that reason depicted in Fig. 10 for the three different stations during the TID occurrence. We can observe that RoTEC is generally in phase for stations ANTW and HERE, which form the baseline showing the smallest positioning error. On the contrary, the AARS and HERE stations, forming the baseline with the largest positioning error, show a temporal shift between their RoTEC values. This time lag due to the TID propagation is thus responsible for the difference in error magnitude observed between the two baselines. These results and those of Table 1 show therefore that the residual ionosphere influence on relative positioning is affected by the baseline orientation during the occurrence of a TID.
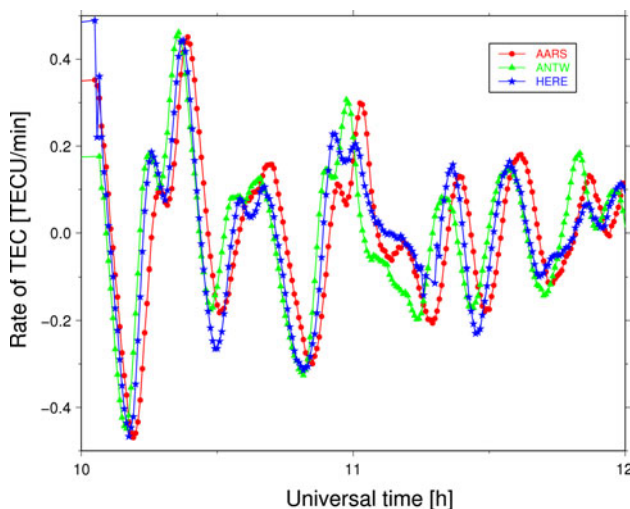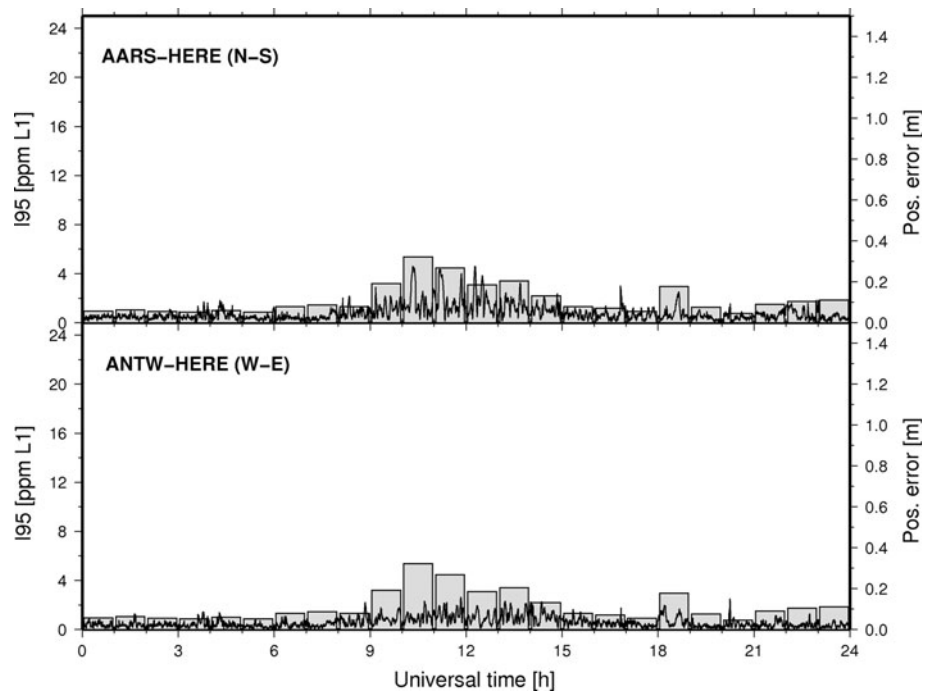
Fig. 10 Rate of TEC (3 min running average) values for stations of AARS, ANTW, and HERE for PRN17 (DOY 359/2004)

DOY 324/2003: Table 1 confirms results relative to the polar plot: the baseline oriented north–south, e.g., DIKS-OOST, presents larger σ and MAX values than the one with east–west orientation (DIKS-PITT). On Fig. 11, we can see that this maximal value of 2.061 m compared to 1.303 m for DIKS-PITT, is observed around 9.30 p.m.

This north–south orientation coincides with the preferential orientation of ionospheric walls during geomagnetic storms, as analyzed by Stankov et al. (2009). They describe the TEC behavior during the occurrence of geomagnetic

storms in the USA and Europe. They show that TEC enhancements due to energy release in polar regions move in the direction of the equator and are followed by a steep TEC depletion. These features correspond to the TEC pattern observed for this day (Fig. 4).

Comparing with I_{95}-index

Figures 9 and 11 give, in addition to ΔB, the I_{95}-index values developed by Wanninger (1999). This index, expressed in ppm on L_1, merges into a single number the ionospheric residual terms I_{AB,L_1}^{ij} relative to all double differences in view in a triangle of GPS permanent stations. This value, valid for all permanent or mobile stations located inside the triangle, gives therefore not only the same value for the two baselines (Fig. 9 or 11) but also for any other baseline located within the particular triangle considered. SoDIPE-RTK produces result taking into account the baseline orientation, contrary to the I_{95}-index. In addition, SoDIPE-RTK offers a better temporal resolution. The I_{95}-index values are obtained hourly while $I_{AB,k}^{ij}$, and thus the positioning error, are computed every 30 s. Therefore, SoDIPE-RTK offers an interesting alternative to I_{95}-index.

Conclusions

Because the ionosphere remains one of the most important error sources in GNSS real-time positioning, it is

Fig. 11 I_{95}-index and positioning error in terms of distance (ΔB) during the occurrence of a severe geomagnetic storm (DOY 324/2003)
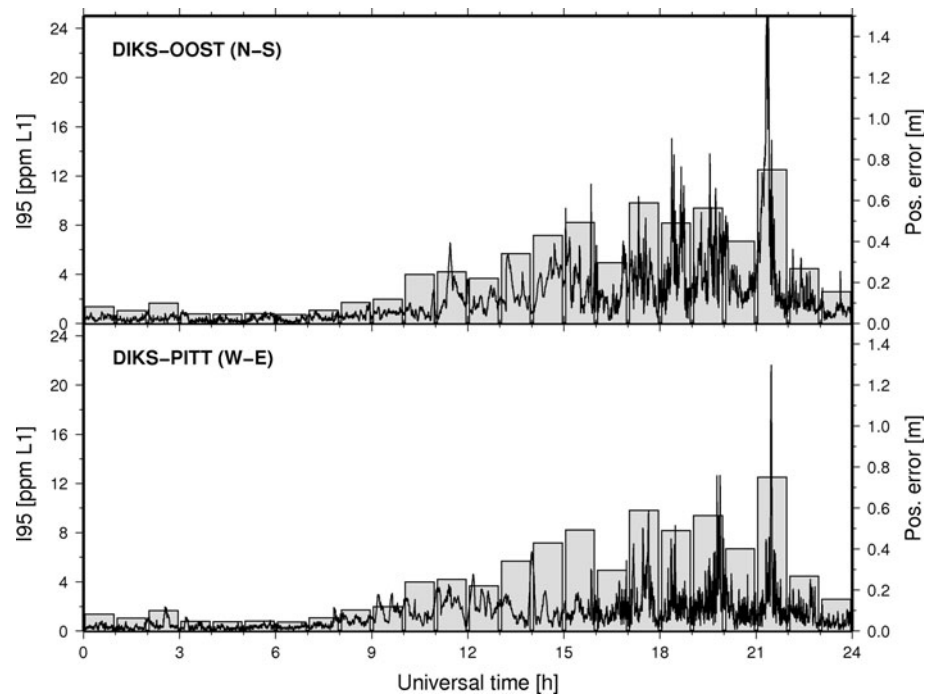
crucial to monitor, model, and forecast the ionospheric activity and its effects on such applications. For this reason, we analyzed the ionospheric variability and its impact on GNSS signals using the SoDIPE-RTK software. For a given baseline, this software solves double-difference ambiguities using the whole observation period and computes the ionospheric positioning error. It thus assesses in a quantitative way the influence of ionospheric small-scale variability on relative GNSS applications. In order to ensure a high-quality and relevant data set, the first part of the work was dedicated to data editing. Each baseline has been carefully screened and edited if necessary to avoid data gaps and outliers. Such a manual editing can be considered as a limitation of the technique. In the future, automated data processing techniques will be implemented. After that preliminary step, for a quiet reference day DOY 310/08 we processed all AGN baselines to validate our methodology. We have observed that the ionospheric residual term induces positioning errors of the same order of magnitude as occur in relative GNSS applications like RTK. The analysis of this day also allowed the assessment, for a given significance level, of the maximum usable baseline length for relative positioning, considering the ionosphere as the only error source. Then, we showed that geomagnetic storms induce larger residuals on positioning than TIDs. For a 20-km baseline, the positioning error reached 0.185 m during a TID (DIKS-PITT, Height component, and DOY 359/04) compared to 0.914 m during a geomagnetic storm (DIKS-PITT, Height component, and DOY 324/03). These values

are obtained for baselines with a specific orientation (east–west). Since the accuracy is also a function of baseline orientation, errors are larger for baselines with a north–south orientation (0.268 m for AARS-HERE Height component on TID day DOY 359/2004 and 1.936 m for AARS-HERE Height component on geomagnetic storm day DOY 324/2003). We observed in these cases that the degradation is due to the preferential direction of TID's propagation. It is therefore important to offer to GNSS users an integrity monitoring service which can help them to take into account the influence of such moving structures. While users are generally aware of the impact of these ionospheric perturbations, they are not especially informed about the propagation of these atmospheric structures. From this point of view, SoDIPE-RTK provides spatial information with a higher resolution than the I_{95}-index. In this regard, polar plots describe in an understandable way the impact of the TIDs propagation and of geomagnetic storms, in terms of structures and gradients. Our research offers an additional, easy to implement method allowing warnings to GNSS users of ionospheric threats. Its improved space–time resolution will help to detect local degradations in RTK positioning error when other indexes such as I_{95} or techniques (VRS, FKP, and MAC) could fail to detect or model them.

References

Brown N, Keenan R, Richter B, Troyer L (2005) Advances in ambiguity resolution for RTK applications using the new RTCM V3.0 master-auxiliary messages. Proceedings of ION GNSS 2005, Long Beach, CA, 73–80

Brown N, Geisler I, Troyer L (2006) RTK rover performance using the master-auxiliary concept. J Glob Position Syst 5:135–144

Chen HY, Rizos C, Han S (2004) An instantaneous ambiguity resolution procedure suitable for medium scale GPS reference station network. Surv Rev 37:396–410

Gende M, Mohino Harris E, Brunini C, Radicella SM, Herraiz M (2005) Ionospheric biases correction for coordinates derived from GPS single point positioning. Ann Geophys, 48:439–444

Gomez L, Sabbione JI, Van Zele MA, Meza A, Brunini C (2007) Determination of a geomagnetic storm and substrom effects on the ionospheric variability from GPS observations at high latitudes. Journal of Atmospheric and Solar-Terrestrial Physics 69:955–968

Hernandez-Pajares M, Juan JM, Sanz J (2000) Application of ionospheric tomography to real-time GPS carrier-phase ambiguities resolution, at scales of 400–1,000 km and with high geomagnetic activity. Geophys Res Lett 27:2009–2012

Hernandez-Pajares M, Juan JM, Sanz J (2006) Medium-scale traveling ionospheric disturbances affecting GPS measurements: spatial and temporal analysis. J Geophy Res, 111:A07S11

Hofmann-Wellenhof B, Lichtenegger H, Collins J (2001) GPS theory and Practice, 5th revised edition, Springer, Wien, NewYork

Janssen V (2009) A comparison of the VRS and MAC principles for network RTK. Proceedings of international global navigation satellite systems society, IGNSS Symposium 2009, Australia

Leick A (2004) GPS satellite surveying third edition. Wiley, New York

Lejeune S, Warnant R (2008) A novel method for the quantitative assessment of the ionosphere effect on high accuracy GNSS applications, which require ambiguity resolution. J Atmos Sol Terr Phys 70:889–900

Mayer C, Jakowski N, Borries C, Pannowitsch T, Belabbas B (2008) Extreme ionospheric conditions over Europe observed during the last solar cycle. In: NAVITEC 2008, ESA/ESTEC, Netherlands

Mohino E (2008) Understanding the role of the ionospheric delay in single-point single-epoch GPS coordinates. J Geodesy 82:31–45

Ou JK, Wang ZJ (2004) An improved regularization method to resolve integer ambiguity in rapid positioning using single frequency GPS receivers. Chin Sci Bull 49:196–200

Saito A, Nishimura M, Yamamoto M, Fukao S, Kubota M, Shiokawa K, Otsuka Y, Ishii M, Sakanoi T, Miyazaki S (2001) Traveling ionospheric disturbances detected in the FRONT campaign. Geophys Res Lett 82:31–45

Stankov SM, Warnant R, Stegen K (2009) Trans-ionospheric GPS signal delay gradients observed over mid-latitude Europe during the geomagnetic storms of October–November, 2003. Adv Space Res 43:1314–1324

Tsugawa T, Saito A (2003) Damping of large-scale traveling ionospheric disturbances detected with GPS networks during the geomagnetic storm, J Geophys Res, 108(A3)

Vollath U, Landau H, Chen X (2002) Network RTK—concept and performance. In: Proceedings of the international symposium on GPS/GNSS, Wuhan, China

Wanninger L (1999) The performance of virtual reference stations in active geodetic GPS-networks under solar maximum conditions. In: Proceedings of ION GPS 99, Nashville TN, USA, p 1419–1427

Warnant R, Pottiaux E (2000) The increase of the ionospheric activity as measured by GPS. Earth Planets Space 52:1055–1060

Wautelet G, Lejeune S, Warnant R (2009) Effects of ionospheric small-scale structures on GNSS. In: Proceedings of IRST 2009, Edinburgh, UK, April, p 196–200